Available online at www.sciencedirect.com
ScienceDirect
International Journal of Heat and Fluid Flow 28 (2007) 441–453
International Journal of HEAT AND FLUID FLOW
www.elsevier.com/locate/ijhff

Experimental study of turbulent cross-flow in a staggered tube bundle using particle image velocimetry

S.S. Paul, M.F. Tachie *, S.J. Ormiston

Department of Mechanical and Manufacturing Engineering, University of Manitoba, Winnipeg, Man., Canada R3T 5V6

Received 15 March 2006; accepted 31 May 2006
Available online 18 July 2006

Abstract

An experimental investigation was performed on turbulent cross-flow in a staggered tube bundle with transverse and longitudinal pitch-to-diameter ratios of 3.8 and 2.1, respectively. A particle image velocimetry technique was employed to obtain detailed measurements in the bundle at inlet-velocity-based Reynolds numbers of 4800, 9300 and 14,400. Quantities reported include mean velocities, turbulence intensities, Reynolds stresses, and various terms in the Reynolds-Averaged Navier–Stokes (RANS) equations. The results reveal higher shear rates in the wake regions. The streamwise and transverse turbulence fluctuations attained peak value of 85% and 105%, respectively, of the approach mean velocity in the wake regions. The flow evolves fairly rapidly and becomes spatially periodic in the streamwise direction after a relatively short distance. The flow exhibits strong Reynolds number dependence in the developing region but no significant Reynolds number effects are observed in the spatially periodic region. The pressure gradient terms in the streamwise and transverse RANS equations are nearly balanced by the Reynolds stress terms in the recirculation zones, and by the convective terms outside the recirculation region.

Keywords: Turbulent flow; Cross-flow; Tube bundle; PIV

1. Introduction

Cross-flow in arrays of cylinders is an active area of research because of its wide practical application to heat exchanger tube bundles, to flow across overhead cables, and to cooling systems for nuclear power plants. There has been a considerable amount of theoretical and experimental work committed to the studies of different aspects of flow around a single cylinder and cylinders in tandem, and to flow in sparse arrays of cylinders. Detailed information about the flow within densely packed cylinder arrays (tube bundles) is, however, limited due to the complexity of the flows and the associated measurement difficulties.

Most of the earlier experimental studies on flows in tube bundles focused on measurement of heat transfer and pressure drop. For example, Pierson (1937), Huge (1937), and Grimson (1937) systematically studied heat transfer and pressure drop in both staggered and in-line tube bundle arrangements of various configurations in cross-flow of gases. Žukauskas and Ulinskas (1998) presented some experimental results as well as extensive discussion on the characteristics of the flow and heat transfer of single tubes and tube bundles in cross-flow. They found that, in the sub-critical flow regime, the pressure drop in a tube bundle decreases with Reynolds number but beyond a critical Reynolds number it increases. They also reported correlations for the total pressure drop and heat transfer coefficients for wide range of Reynolds numbers and tube bundle configurations.

A number of flow visualization studies have been performed to obtain flow patterns in tube bundles. Wallis (1939) was among the first to perform one of these studies, which he carried out for the free surface flow through both staggered and in-line configurations with Reynolds numbers ranging from 132 to 2700. He reported that attached

* Corresponding author. Tel.: +1 204 4749589; fax: +1 204 2757507.
E-mail address: tachiemf@cc.umanitoba.ca (M.F. Tachie).

0142-727X/$ - see front matter © 2006 Elsevier Inc. All rights reserved.
doi:10.1016/j.ijheatfluidflow.2006.06.001

Nomenclature

d	tube diameter (m)	$-\langle uv\rangle$	Reynolds shear stress ($m^2\ s^{-2}$)
l_r	recirculation length (m)	V	y-direction mean velocity component ($m\ s^{-1}$)
P	pressure ($N\ m^{-2}$)	v	y-direction velocity fluctuation ($m\ s^{-1}$)
Re_∞	Reynolds number based on the inlet velocity ($=U_\infty d/\nu$)	$\langle vv\rangle$	normal Reynolds stress along the y-axis ($m^2\ s^{-2}$)
S_L	longitudinal pitch (m)	W	z-direction mean velocity component ($m\ s^{-1}$)
S_L^*	longitudinal pitch-to-diameter ratio ($=S_L/d$)	x	streamwise coordinate (m)
S_T	transverse pitch (m)	y	transverse coordinate (m)
S_T^*	transverse pitch-to-diameter ratio ($=S_T/d$)	z	span-wise coordinate (m)
U	x-direction mean velocity component ($m\ s^{-1}$)	*Greek symbols*	
U_∞	approach velocity ($m\ s^{-1}$)	ρ	fluid density ($kg\ m^{-3}$)
u	x-direction velocity fluctuation ($m\ s^{-1}$)	ν	kinematic viscosity ($m^2\ s^{-1}$)
$\langle uu\rangle$	normal Reynolds stress along the x-axis ($m^2\ s^{-2}$)	ρ_{uv}	correlation coefficient ($=\langle uv\rangle/\sqrt{\overline{u^2}}\sqrt{\overline{v^2}}$)

eddies were formed alternatively behind each of the cylinders on either side. These eddies were occasionally dragged into the main stream. It was also observed that an increase in the transverse pitch reduced the mean velocity both in the main stream and in the wake. Weaver and Abd-Rabbo (1985) performed a flow visualization study of flow in in-line and square arrays with a pitch-to-diameter ratio of 1.5. Periodic vortex shedding was observed. Detailed reviews of flow visualization have been presented by Beale and Spalding (1999), Sweeney and Meskell (2002) and Polak and Weaver (1995). A few measurements in a tube bundle using hot-wire anemometry have been reported. Aiba et al. (1982a,b) performed mean and turbulent intensity measurements in in-line and staggered tube bundles using a two-component hot-wire anemometer. The pitch ratios were varied from 1.2 to 1.6 and the Reynolds number varied from 30,000 to 40,000.

A high level of turbulence and regions of flow reversal characterize turbulent flow through tube bundles. For these reasons, laser Doppler anemometry (LDA) and particle image velocimetry (PIV) are suitable for studying turbulent flow through tube bundles. Table 1 summarizes some of the pertinent experimental studies performed using LDA and PIV. Simonin and Barcouda (1986) performed LDA measurements in a tube bundle. They observed a small recirculation zone in the wakes of tubes and fairly high turbulence intensity values. In a subsequent study in the same tube bundle arrangement, Simonin and Barcouda (1988) performed LDA measurements up to the sixth row. It was observed that the length of the recirculation zone is highest behind the first row and decreases in subsequent downstream rows. Halim (1988) performed LDA measurements both in staggered and in-line geometries. Halim found higher transverse mean velocities in the staggered array but the turbulence levels in both geometries were similar. Meyer (1994) also employed LDA to measure two-dimensional mean velocities and Reynolds stresses in two successive rows in the middle of tube bundle. The measurements were compared with predictions using both a standard k–ε model and the second moment closure proposed

Table 1
Summary of previous experimental studies performed using LDA and PIV

Author(s)	Reynolds number	Arrangement: $S_T^* \times S_L^*$	Rows	Tubes per row	Quantities measured
Simonin and Barcouda (1986)	$Re_\infty = 20{,}000$	S: 2.074×1.037	S: 7	S: 10 or 11	U, V, $\langle uv\rangle$ and k
Simonin and Barcouda (1988)	$Re_\infty = 18{,}000$	S: 2.074×1.037	S: 7	S: 10 or 11	U, V, $\langle uv\rangle$ and k
Halim (1988)	$Re_{max} = 60{,}000$–$100{,}000$	S: 1.58×1.58 I: 1.745×1.745	S: 5 I: 6	S: 3 or 4 I: 3	U, V, u, v and $\langle uv\rangle$
Meyer (1994)	$Re_{max} = 32{,}000$	S: 2.0×1.0	S: 9	S: 3 or 5	U, V, $\langle uu\rangle$, $\langle vv\rangle$, $\langle uv\rangle$ and local heat transfer
Balabani and Yianneskis (1996)	$Re_{max} = 12{,}858$	S: 3.6×1.6 S: 3.6×2.1 I: 3.6×2.1	S: 6 I: 5	S: 3 or 2 I: 3	U, V, u, v, ε, pressure drop, turbulence scales and spectra
Iwaki et al. (2004)	$Re_\infty = 1260$–6933	S: 1.5×0.75 I: 1.5×1.5	S: 20 I: 20	S: 5 or 4 I: 5	u, v, velocity vector and vortex structure

S = Staggered, I = In-line, Re_∞ = Reynolds number based on U_∞ and Re_{max} = Reynolds number based on U_{max}. All studies except Iwaki et al. (2004) used LDA; Iwaki et al. (2004) used PIV.

by Launder et al. (1975). It was observed that both models gave poor predictions of the Reynolds stresses. Balabani et al. (1994) employed an LDA to measure mean velocities and turbulent intensities in a staggered tube bundle. Based on the approach velocity and tube diameter, the Reynolds number is equal to 9280. The results were compared to a standard k–ε turbulence model with and without a curvature modification. In a later work, Balabani and Yianneskis (1996) performed flow measurements using three tube bundle configurations with a large pitch-to-diameter ratio: two staggered arrangements and one in-line arrangement. In each row, two half tubes were also mounted along the top and bottom walls of the test model. In all cases the tube diameter was 10 mm. Recently, Iwaki et al. (2004) employed a PIV method to study the flow field in tube bundles arrangements. The Reynolds-Averaged Navier–Stokes (RANS) with different turbulence models and Large Eddy Simulation (LES) have been used in the past to predict turbulent flow in tube bundles. For example, Rollet-Miet et al. (1999) employed LES and a k–ε model to predict the experiments of Simonin and Barcouda (1988). Both the LES and the k–ε model predicted the mean velocity profiles reasonably well. In contrast to the LES results, however, the k–ε model gave poor prediction of the Reynolds stresses in the wake region. As noted earlier, other numerical results obtained using a k–ε model and the second moment closure proposed by Launder et al. (1975) as well as a standard k–ε turbulence model with and without a curvature modification did not compare well with experiments. The shortcomings of these turbulence models may be partly explained by the differences between the flow field in tube bundle and the generic flows used to calibrate the turbulence models.

In the present work, a PIV method is used to conduct detailed velocity measurements in turbulent flow in a staggered tube bundle. The measurements were performed at three Reynolds numbers to study the effects of Reynolds number on the time-averaged mean and turbulence statistics. The Reynolds numbers based on the inlet velocity were $Re_\infty = 4800$, 9300 and 14,400. The intermediate Reynolds number ($Re_\infty = 9300$) was chosen to facilitate detailed comparisons of the present work with the LDA measurements of Balabani and Yianneskis (1996) at $Re_\infty = 9280$. The lowest Reynolds number was constrained by the minimum velocity that could be achieved in the tunnel. The maximum Reynolds number was chosen to be approximately 1.5 times the intermediate Reynolds number. Streamlines, profiles of mean velocity, turbulence intensities and Reynolds stresses as well as various terms in the Reynolds-Averaged Navier–Stokes equations are used to examine the salient features of the flow.

2. Experimental setup and measurement procedure

The experiments were conducted in a closed-circuit water tunnel. The tunnel was designed and constructed at the Engineering Laboratory Design, Inc., Minnesota, USA. Fig. 1a shows a schematic diagram of the water tunnel. The sidewalls and floor of the test section are made of abrasion-resistant clear acrylic to facilitate optical access. The settling chamber upstream of the contraction section is fitted with perforated steel plates and a honeycomb section to condition the flow. A contraction with a six-to-one area ratio and a symmetrical cross-section is used to further reduce the turbulence intensity by accelerating the mean flow. The interior dimensions of the test section are 200 mm wide by 200 mm high by 2500 mm long. The test section is provided with two removable lids made of acrylic sheet. This enables the water tunnel to be operated either as a closed or an open channel. The pump is belt-driven by a 25 hp, 600 V A/C 3-phase 60 Hz motor. A Toshiba transistor inverter type, variable speed motor control regulates the speed of the motor that drives the pump. The system is also furnished with a filter system that removes dye concentrations and other unwanted particles from the working fluid when the need arises. Fig. 1b shows details of the test section with the tube bundle, a charged-coupled device (CCD) camera and a laser arrangement.

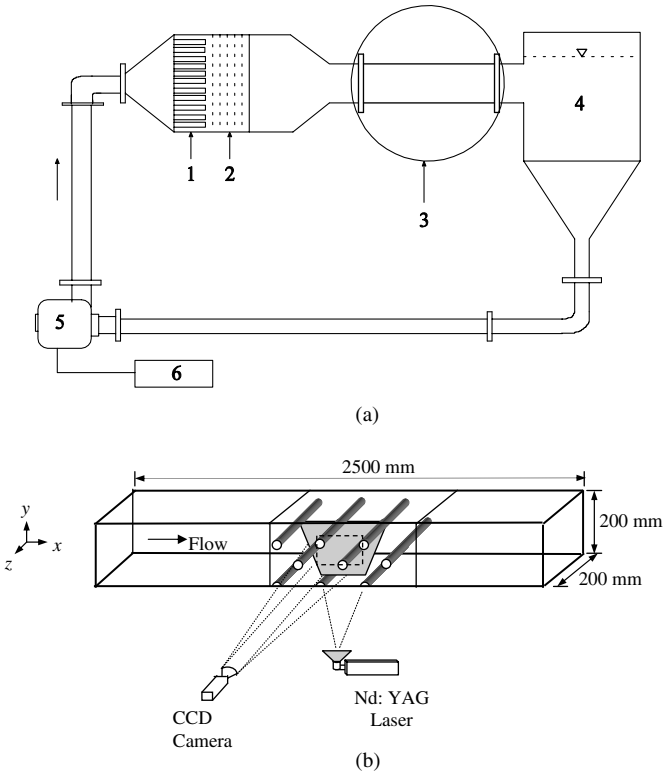

Fig. 1. Experimental setup: (a) schematic of the water tunnel: 1 – honeycomb, 2 – perforated plate, 3 – test section, 4 – tank, 5 – pump, and 6 – variable speed controller, and (b) test section including a CCD camera and a laser arrangement.

The flow was seeded with polyamide particles having a mean diameter of 5 μm and specific gravity of 1.03. The settling velocity and response time of the particles were estimated to be 0.41 μm/s and 1.43 μs, respectively (for all the experiments). The settling velocity is small compared to the mean axial velocity measured and the response time is very small compared to the sampling time of about

700 μs. Therefore, the particles are considered to follow the fluid faithfully. An Nd-YAG, 120 mJ pulse laser of 532 nm wavelength was used to illuminate the flow field. The laser sheet was located at the mid-plane of the channel and positioned perpendicularly to the camera as shown schematically in Fig. 1b. A 60 mm diameter Nikkor lens fitted to a high-resolution digital camera (Dantec Dynamic HiSense 4 M camera) that uses a CCD with 2048×2048 pixels and a 7.4 μm-pixel pitch. The measurements were made at a field of view of 200×200 mm. The images were acquired continuously through a buffer system onto a 3.0 GHz Pentium 4 computer with 1 Gb RAM and two 250 Gb hard drives using Dantec Dynamics' FlowManager software running on Windows XP. The images acquired were processed by the adaptive correlation option of commercial software developed by Dantec Dynamics with a 32×32 pixels interrogation window, 50% overlap and moving average validation. The adaptive correlation uses a multi-pass FFT cross-correlation algorithm to determine the average particle image displacement within an interrogation window. A three-point Gaussian is used for the determination of particle image displacement with sub-pixel accuracy. The mean flow and turbulence statistics were computed using a Matlab script written in our lab.

Fig. 2a shows a sectional side-view of the tube bundle model used. The bundle consists of six rows of tubes of outer diameter of 25.4 mm arranged in a staggered array. As shown in the figure, each row has 1 or 2 full tubes. Half tubes were also mounted along the top and bottom walls of the test model alternately to simulate an infinite tube bundle and minimize the wall boundary layer. The transverse and longitudinal pitch-to-diameter ratios, S_T^* and S_L^*, were 3.8 and 2.1, respectively. The length-to-diameter ratio of the rods was 7.5 so that measurements obtained at the mid-span could be considered free from end effects. Also shown in Fig. 2a is the coordinate system used and key geometrical parameters. The origin of the coordinate system is defined to be at the center of the middle tube in the first row. Here, the streamwise and transverse directions are denoted by x and y, respectively. The z-axis (span-wise), not shown, is assigned to the direction pointing out of the paper. The experiments were performed at Reynolds numbers of 4800, 9300 and 14,400. These values are based on the tube diameter ($d = 25.4$ mm) and approach velocities in the water tunnel of 0.19 m/s, 0.37 m/s and 0.57 m/s. Fig. 2b shows the details of the region where most results will be presented using spatial coordinates normalized by the tube diameter. The majority of the results will be presented at the following x/d locations: 0.85, 1.25, 2.95, 3.35, 5.05, 5.45, 7.15 and 7.55 in the region $0.0 \leqslant y/d \leqslant 1.9$, as indicated in Fig. 2b. Some of the results will be presented at $y/d = 0$ in the region $0.0 \leqslant x/d \leqslant 8.0$, which is also shown in Fig. 2b. The approach velocity, U_∞, will be used to normalize both the mean velocities and the turbulence quantities. It must be noted that in the presentation of some results, some of the data points were skipped for clarity.

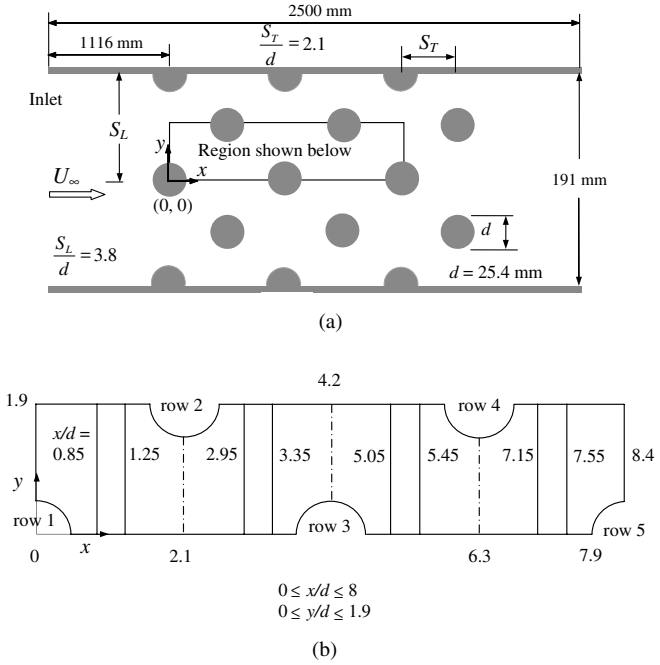

Fig. 2. (a) Cross-sectional view of the tube bundle model with the definition of geometrical parameters and the coordinate system used, and (b) locations at which results are presented: $x/d = 0.85$, 1.25, 2.95, 3.35, 5.05, 5.45, 7.15 and 7.55.

Preliminary measurements were conducted to determine the sample size required to achieve statistically converged results for the mean flow and turbulence statistics. Based on the results, a sample size of 3000 was used to compute those statistics in this work. Detailed measurements were made upstream of the tube bundle to characterize the approach boundary layer. At $x/d = -10$, it was found that the mean velocity is uniform across the central 70% of the channel with a boundary layer thickness of 34 mm. The streamwise and transverse turbulence intensities in the central portion of the channel were 4% and 3%, respectively.

The uncertainty analysis of the present measurement follows the AIAA standard derived and explained by Coleman and Steele (1995). In general, a complete uncertainty analysis involves identifying and quantifying both the bias and precision errors in each part of the measurement chain. In PIV techniques, the accuracy of velocity measurement is limited by the accuracy of the sub-pixel interpolation of the displacement correlation peak. Other sources of measurement uncertainties include particle response to fluid motion, light sheet positioning, light pulse timing and size of interrogation area. Detailed analyses of bias and precision errors inherent in PIV techniques are available in Prasad et al. (1992), Westerweel (1997) and Forliti et al. (2000). Forliti et al. (2000) have shown that a Gaussian peak-fitting algorithm has the lowest bias and precision errors. On the basis of the size of interrogation area and curve fitting algorithm used to calculate the instantaneous vector maps, and the large number of instantaneous vector maps used to calculate the mean velocity and turbulent quanti-

ties, we estimate the uncertainty in the mean velocities at 95% confidence level to be ±3%. The uncertainties in turbulence intensities and Reynolds stresses are estimated to be ±7% and ±10%, respectively. Close to the tubes, uncertainties in mean velocities and Reynolds stresses are estimated to be ±5% and ±12.5%, respectively. The uncertainties in the first derivatives are of the order of ±15%. The positions of the cylinder above the wall surfaces were set with an accuracy of ±0.5 mm.

3. Results and discussion

3.1. Streamlines and mean velocity across the tube bundle

The streamlines are generated using PIV software developed by Dantec Dynamics. The streamlines of the flow measured over the first four rows of tubes at $Re_\infty = 9300$ are shown in Fig. 3. The streamlines are nearly symmetric about the center line ($y = 0$) of the bundle. Two vortices, similar in size, nearly symmetrical about the tubes' horizontal center line, and opposite in rotational direction, are formed downstream of the first tube row. Similar features were observed with less intensity behind the second row of tubes but tend to disappear beyond the second row. This finding is consistent with that of Balabani and Yianneskis (1996). It is interesting to note that the flow pattern in the first row is qualitatively similar to that of an isolated single cylinder in cross-flow.

In order to provide insight into the behavior of the flow through successive rows in the bundle, data were obtained at $x/d = 1.25$, 3.35, 5.05 and 7.55 in the region $-3.8 \leqslant y/d \leqslant 3.8$. The streamwise and transverse mean velocities at these locations are shown in Fig. 4. It is clear from Fig. 4a that the profiles of the streamwise mean velocity are symmetric about $y = 0$. The magnitude of the peak velocity in the wake behind the first tube is approximately

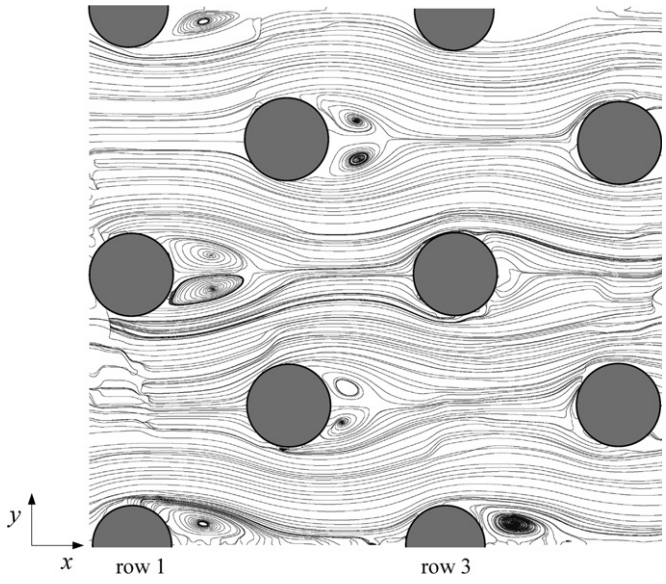

Fig. 3. Streamlines for the first four rows of the bundle for $Re_\infty = 9300$.

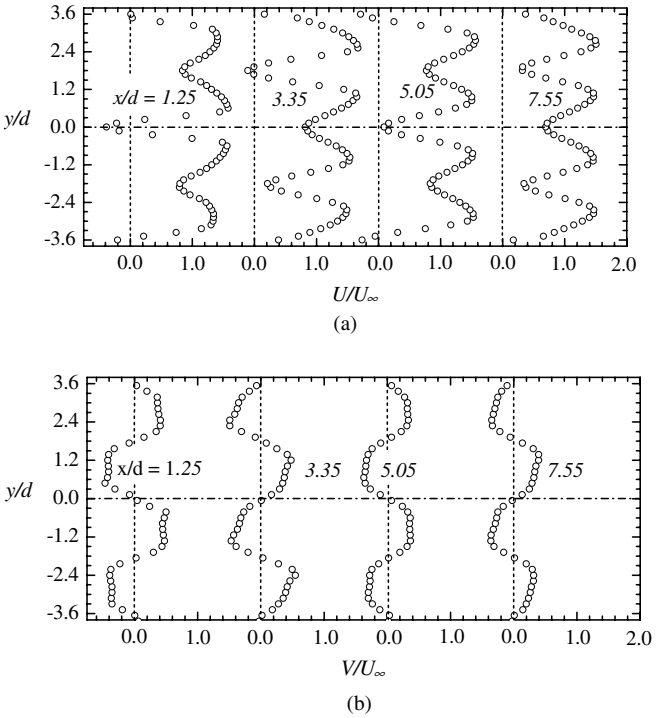

Fig. 4. Profiles of non-dimensional mean velocity across the entire height of the bundle: (a) U/U_∞ and (b) V/U_∞ at selected x/d locations.

40% of the approach velocity. The magnitude of the peak velocity behind the second row reduces to about 10% of the approach velocity and this magnitude tends to reduce further in the subsequent rows. As shown in Fig. 4b, the transverse mean velocity is anti-symmetric with respect to $y = 0$. Changes in the orientation of the profiles are observed at successive rows. Adjacent rows (e.g., the profiles at $x/d = 5.05$ and 7.55) are mirror images of each other with respect to $y = 0$. The profile at $x/d = 3.35$ shows that V can be as high as 0.6 U_∞. This implies significant mean motion in the transverse direction.

The symmetry noted above is consistent with the studies of Halim (1988), Simonin and Barcouda (1988) and Balabani and Yianneskis (1996). Because of the symmetry and also to facilitate comparison with the results of Balabani and Yianneskis (1996), all subsequent presentation of results is restricted to the region indicated in Fig. 2b.

3.2. Mean velocity and turbulence intensities along the center line

Fig. 5 shows values of streamwise mean velocity along the center line ($y = 0$) of the bundle. The distribution of the streamwise component of the mean velocity along the wake center line provides information about the recovery of the streamwise mean velocity as well as the length of the recirculation zone. Balabani and Yianneskis (1996) defined the recirculation length, l_r, as the distance between the tube rear surface and the point of zero streamwise mean velocity. This corresponds to the distances between points

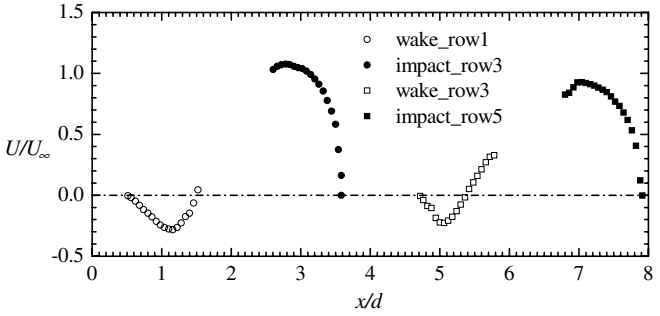

Fig. 5. Profiles of non-dimensional mean velocity, U/U_∞, along the center line of the bundle.

$x/d = 0.5$ and 1.5 and between $x/d = 4.7$ and 5.4 in curves wake_row1 and wake_row3, respectively, in Fig. 5. Fig. 5 also reveals regions of high velocities between successive tube rows and low negative velocities in the wakes of the tubes. Along the center line behind a tube the value of U/U_∞ decreases with a minimum occurring at about the center of the recirculation zone, after which it rises to zero at the end of the recirculation zone.

The values of the recirculation length, l_r, obtained downstream of the first and third rows in the present study and by Balabani and Yianneskis (1996) and Iwaki et al. (2004) are shown in Table 2. It should be noted that the values reported by Balabani and Yianneskis (1996) were obtained at $Re_\infty = 9280$ and their pitch ratios are similar to those in the present study. Iwaki et al. (2004) measured l_r behind the first four rows of a tube bundle of smaller pitch ratios and over a range of Reynolds numbers. They observed that values of l_r are nearly independent of location and of Reynolds number. In the present study, a value of $l_r = 1.0d$ was obtained behind the first row at the three Reynolds numbers studied. The values of l_r obtained downstream of the third row vary only slightly with Reynolds number. The present value of $l_r = 1.0d$ behind the first row is higher than $l_r = 0.8d$ obtained by Iwaki et al. (2004). It is, however, lower than $l_r = 1.3d$ obtained by McKillop and Durst (1984) behind a single circular cylinder at a similar Reynolds number and $l_r = 1.3d$ obtained by Balabani and Yianneskis (1996) at a similar location.

Table 2
Summary of recirculation length values obtained in the present and previous studies

Authors	Re_∞	Row	l_r/d
Present study	4800	1	1.0
		3	0.6
	9300	1	1.0
		3	0.7
	14,400	1	1.0
		3	0.8
Balabani and Yianneskis (1996)	9280	1	1.3
		3	0.65
Iwaki et al. (2004)	1260–6933	1	0.8
		3	0.8

The value of $l_r = 0.7d$ downstream of the third row in the present study at $Re_\infty = 9300$ compares very well with $0.65d$ and $0.8d$ reported by Balabani (1996) and Iwaki et al. (2004), respectively, at a similar location. It appears, from the limited comparison, that the value of l_r behind the first row depends on the pitch ratio and possibly the upstream flow conditions.

The minimum normalized streamwise velocities values in region wake_row1 for $Re_\infty = 4820$, 9300 and 14,400 are −0.08, −0.28 and −0.37, respectively. The corresponding values in region wake_row3 are −0.28, −0.23 and −0.17, respectively. In this range of Reynolds numbers, therefore, an increase in the Reynolds number produces an increase in the magnitude of the minimum velocity in region wake_row1. In region wake_row3, however, an increase in the Reynolds number is accompanied by a decrease in magnitude of the minimum velocity.

In Fig. 5 it is also observed that the maximum values of U/U_∞ along $y = 0$ occur in regions impact_row3 and impact_row5. These maxima for region impact_row3 are 1.01, 1.08 and 1.20 for $Re_\infty = 4820$, 9300 and 14,400, respectively. The corresponding maxima for region impact_row5 are 0.83, 0.93 and 1.05, respectively. The value of U/U_∞ decreases to zero at the front face of the next tube (i.e., at $x/d = 3.7$ and 7.9). The near-peak U values in region impact_row5 are 12–18% lower than the corresponding values in the impact_row3 region. These results also reveal the Reynolds number dependence of the streamwise mean velocity in impact regions.

Fig. 6 shows the variation of the turbulent intensities in the streamwise and transverse directions along $y = 0$ at

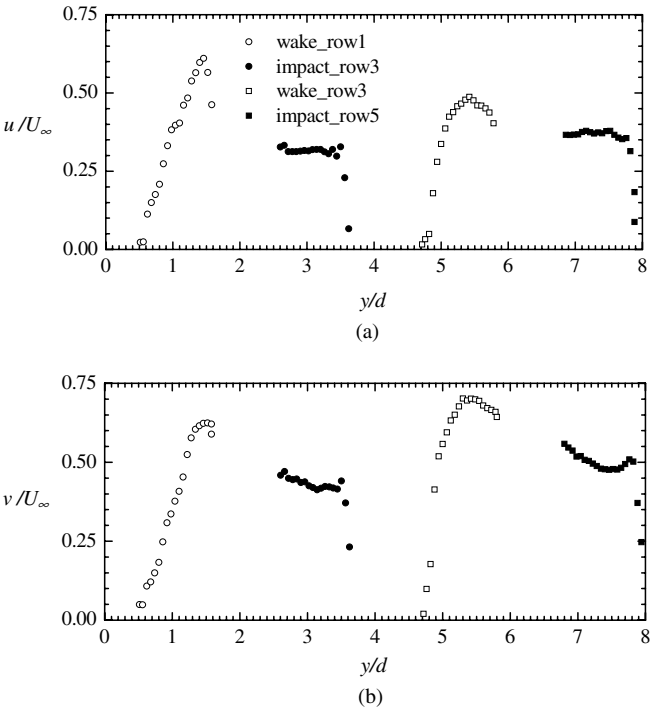

Fig. 6. Profiles of non-dimensional turbulence intensity: (a) u/U_∞ and (b) v/U_∞ along the center line of the bundle.

$Re_\infty = 9300$. Fig. 6a shows that in the wake region downstream of the first row, the magnitude of u/U_∞ increases sharply with distance to a maximum value of about $0.6U_\infty$. This is followed by a gradual decrease to a constant value of about $0.3U_\infty$ behind the second row, and a sharp decrease to approximately zero at the front face of the next tube. Similar trends are also observed between the third and fifth rows but with a maximum value of about $0.5U_\infty$. The profiles of v/U_∞ plotted in Fig. 6b show similar trends to those in Fig. 6a, except that values of v/U_∞ are relatively higher than u/U_∞ at corresponding locations. The high turbulent levels observed in Fig. 6 are indicative of significant mixing along the center line, especially in the recirculation region. The results also clearly show a relatively higher turbulent mixing process in the transverse direction than in the streamwise direction.

3.3. Mean velocity derivatives and profiles

The derivatives of the mean velocities play an important role in the transport of momentum, Reynolds stresses and turbulent kinetic energy. They can also be used to evaluate departure of the mean flow from two-dimensionality and the so-called thin-layer assumptions. For these reasons, the velocity gradients $\partial U/\partial x$, $\partial V/\partial y$, $\partial U/\partial y$ and $\partial V/\partial x$ were evaluated. The velocity gradients were estimated using central differencing. The profiles of the gradients of the mean velocities at selected x/d locations are shown in Fig. 7. Note that the velocity gradients are normalized by the tube diameter (d) and the approach velocity (U_∞). The x-axis range for the repeated sections in Fig. 7 is 0–10. Steep velocity gradients are observed in the recirculation zones. This finding is consistent with that of Simonin and Barcouda (1986). It is observed that the mean velocity gradients have maxima in the recirculation regions and are often much smaller in magnitude outside these regions. The profiles indicate that $(d/U_\infty)(\partial U/\partial x) \approx (d/U_\infty)(-\partial V/\partial y)$ at the selected x/d locations. This suggests that $(d/U_\infty)(\partial W/\partial z) \approx 0$ from continuity. Therefore, it can be concluded that the mean flow in the mid-plane of the bundle is approximately two-dimensional. Fig. 7 demonstrates that the magnitude of $\partial U/\partial y$ is generally higher than the other terms. In the recirculation region, $\partial U/\partial x$ is predominantly positive and $\partial V/\partial y$ is generally negative. On the other hand, the sign of $\partial U/\partial y$ in the recirculation regions changes to conform to the direction of vortex rotation and position of the tubes. Although $\partial U/\partial x$ and $\partial V/\partial y$ are smaller than $\partial U/\partial y$, they are generally not negligible. Thus, the importance of $\partial U/\partial x$ and $\partial V/\partial y$ in the transport equations cannot be neglected.

The present streamwise and transverse mean velocities at various x/d locations for a Reynolds number of 9300 are compared with those of Balabani and Yianneskis (1996) at $Re_\infty = 9280$ in Figs. 8 and 9, respectively. The

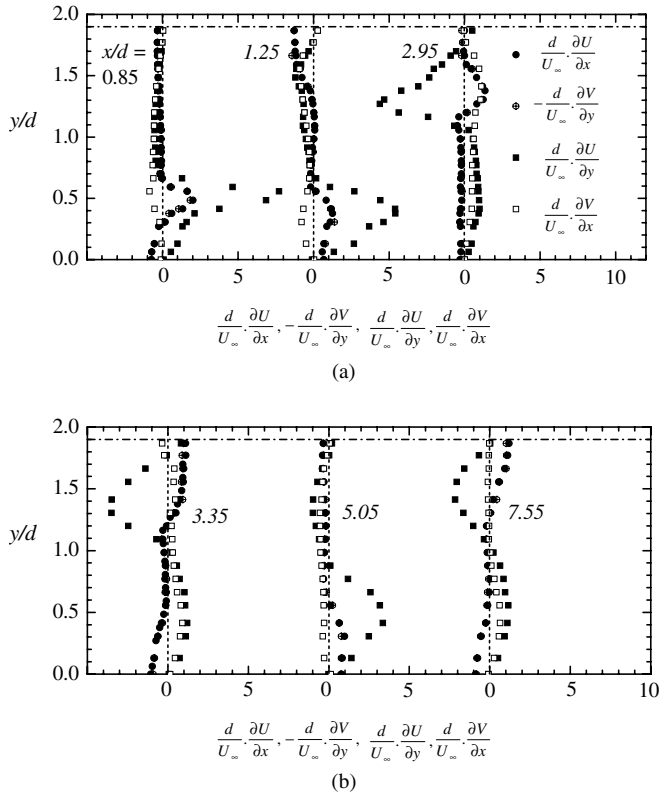

Fig. 7. Profiles of dimensionless velocity gradients at selected x/d locations.

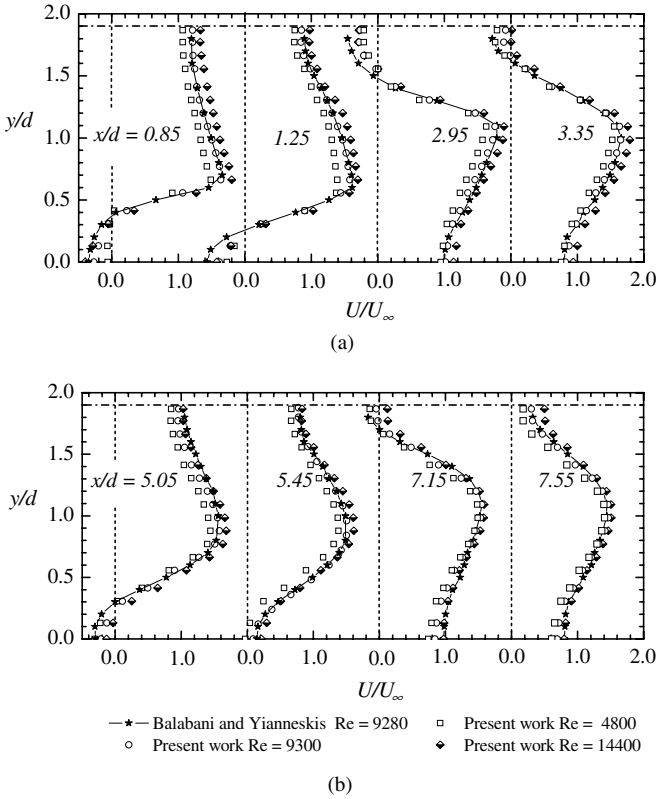

Fig. 8. Profiles of non-dimensional streamwise mean velocity, U/U_∞, at selected x/d locations.

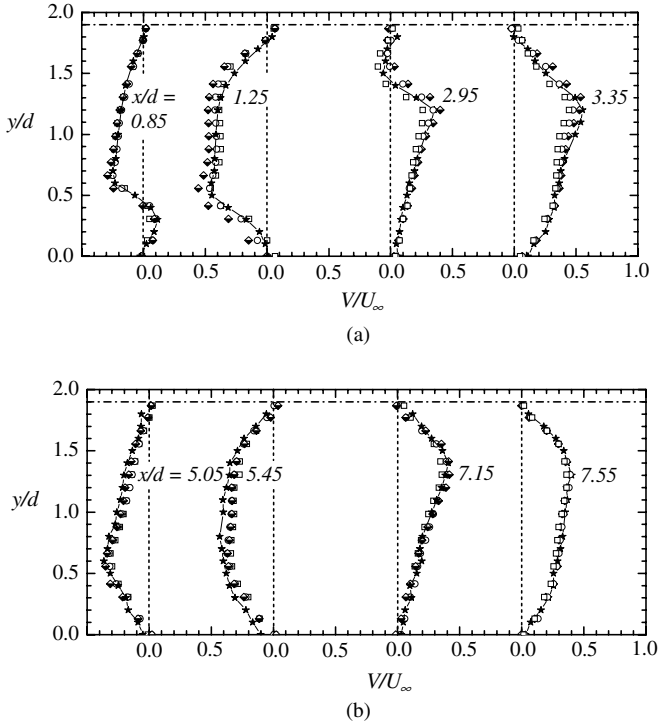

Fig. 9. Profiles of non-dimensional transverse mean velocity, V/U_∞, at selected x/d locations; symbols same as in Fig. 8.

figures also include the present results obtained at Reynolds numbers of 4800 and 14,400. In Fig. 8, the x-axis range is from 0.0 to 2.0 for each repeating section. Fig. 8a shows that the streamwise mean velocities at $x/d = 0.85$ to 3.35 increase from negative values in the recirculation regions to maxima and then decrease to a value of approximately unity. The maximum values occur at the minimum flow cross-sectional areas. Similar trends are observed at $x/d = 5.05$–7.55 (Fig. 8b). The negative values, however, become less significant after $x/d = 5.05$. Flow reversal is therefore most pronounced downstream of the first two rows, and thereafter it appears to be less evident. The profiles in Fig. 8b all have similar maximum values of about $1.6U_\infty$. There is a good agreement of the mean streamwise velocities with those of Balabani and Yianneskis (1996). The figures also reveal no significant change in the distribution of the mean velocities with Reynolds number.

The x-axis range for the repeated sections in Fig. 9 is 0.0–1.0. At $x/d = 0.85$ and 1.25 (Fig. 9a), V velocity is mainly negative (except in the recirculation zone behind row 1) because the flow is moving into the gap below row 2. The velocity is mainly positive at $x/d = 2.95$ and 3.35 because the flow is moving into the gap above row 3. These same trends are also observed between the fourth and the fifth rows. In general, the peaks of the profiles of V in Fig. 9 have lower magnitudes than those in Fig. 8. There is a good agreement of the mean transverse velocities with those of Balabani and Yianneskis (1996). The data also reveal no significant change in the distribution with Reynolds number.

3.4. Turbulent intensities and Reynolds shear stress

Figs. 10 and 11 show profiles of the streamwise and transverse components of the turbulence intensity at the three Reynolds numbers studied. The x-axis range of repeated section in both figures is 0–1. The figures indicate that the distributions of the streamwise and transverse turbulence intensities are qualitatively similar. In addition, the profiles of both components have their peak values in the recirculation regions. The values of the streamwise component are generally much smaller than those of the transverse component at all locations, signifying more intense transverse mixing. This observation is different from results obtained in classical turbulent boundary layers and two-dimensional channels where the streamwise turbulence intensity is generally higher than the transverse turbulence intensity. Fig. 10 shows that, for $Re_\infty = 9300$, the streamwise turbulence intensity rises from about $0.4U_\infty$ in the recirculation region of the first row to a maximum value of $0.85U_\infty$ in the recirculation region shown at $x/d = 3.35$. This significant increase was not found downstream of the third and subsequent rows (Fig. 10b). In Fig. 11, the profiles of the transverse intensity reveal that a maximum value of $1.05U_\infty$ is attained in the recirculation region of the second row (Fig. 11a) for $Re_\infty = 9300$. From these results, it can be inferred that mixing reached its maximum at a relatively short distance in the tube bundle. The production term in the transport equation for $\langle vv \rangle$ can be used to explain the high values of v observed in Fig. 11.

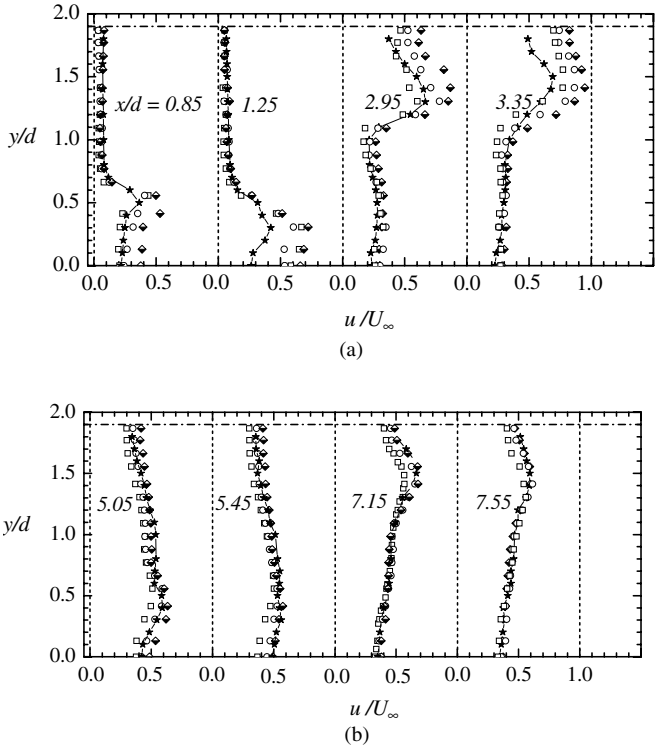

Fig. 10. Profiles of non-dimensional streamwise turbulence intensity, u/U_∞, at selected x/d locations; symbols same as in Fig. 8.

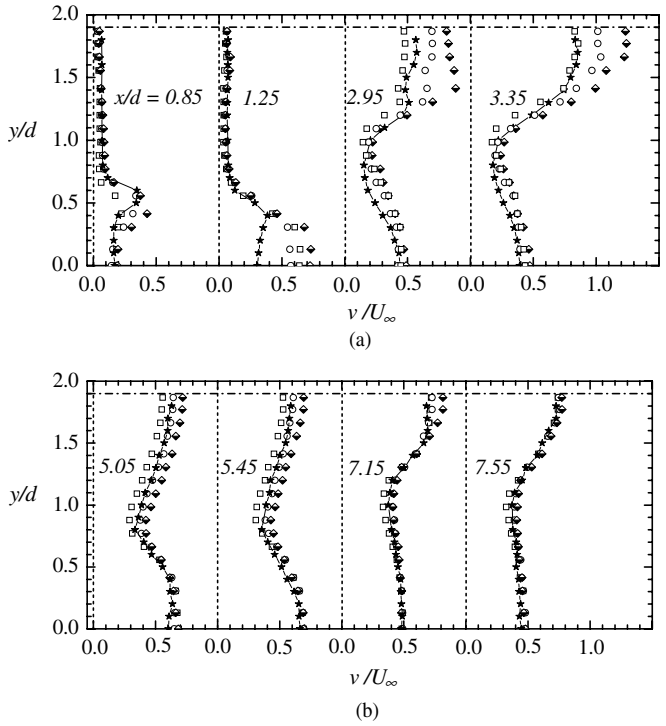

Fig. 11. Profiles of non-dimensional transverse turbulence intensity, v/U_∞, at selected x/d locations; symbols same as in Fig. 8.

The transport equations for the Reynolds stresses can be found in many text books on turbulence, for example, Hinze (1975), and also in Leschziner (2006). It was observed in Fig. 7 that $\partial V/\partial y$ is predominantly negative in the recirculation regions. Our analysis showed that the magnitude of $-\langle uv\rangle\partial V/\partial x$ is negligible compared to $-\langle vv\rangle\partial V/\partial y$. Therefore, $-\langle vv\rangle\partial V/\partial y$ is the dominant production term in the transport equation for $\langle vv\rangle$. Since $\langle vv\rangle$ is always positive, $-\langle vv\rangle\partial V/\partial y$ will make a positive contribution to the production term in the $\langle vv\rangle$ equation. This gain in production of $\langle vv\rangle$ may partly explain the relatively higher values of the transverse turbulence intensity in the recirculation region.

Figs. 10 and 11 indicate some variation in the turbulent intensity profiles obtained at various Reynolds numbers only in the wake regions. Outside the wakes, the profiles nearly collapse on each other. The variation of these profiles with Reynolds number is dramatic in the region $x/d \leqslant 3.35$ and only moderate in the region $x/d > 3.35$. It, therefore, appears from these trends that the turbulent intensity shows a significant Reynolds number effect in the region $x/d \leqslant 3.35$ but a weak Reynolds number dependence at $x/d > 3.35$. The results also show that the present profiles obtained at $Re_\infty = 9300$ are higher than the data reported by Balabani and Yianneskis (1996) at a similar Reynolds number in the region $x/d \leqslant 3.35$. This may be due to differences in tube bundle geometry and upstream conditions in both studies. Beyond $x/d = 3.35$, the present profiles collapse reasonably well with those of Balabani and Yianneskis (1996). These results show that the turbulent intensity profiles in the developing region ($x/d \leqslant 3.35$) are sensitive to Reynolds number and differences in geometry and upstream conditions.

The profiles of Reynolds shear stress at selected x/d locations are shown in Fig. 12. It is interesting to note that the magnitude of the Reynolds shear stress is relatively lower outside the recirculation regions. The profiles of $-\langle uv\rangle$ in the regions behind the first two rows have single peaks in the recirculation zone. Thereafter, the profiles have double peaks, one in the recirculation zone and the other in the passage between rows of tubes. At each x/d location, the peak in the recirculation region is relatively higher than the corresponding one in the passage between the rows of tubes. It is interesting to note that as the flow evolves through the bundle, the peak values in the recirculation regions increase initially to a maximum value at $x/d = 3.35$ and then remain approximately constant. It is also noteworthy that the profiles of $\partial U/\partial y$ in Fig. 7 and $-\langle uv\rangle$ in Fig. 12 show similar trends. The change in the orientation of the upper and lower portions of the $\langle uv\rangle$ profiles at successive rows is due to the direction of vortex rotation and position of the tubes. The local maximum in the recirculation region corresponds to the vortex formation section where $\partial U/\partial y$ is also maximum. It appears that the bulk of $-\langle uv\rangle$ is produced in the wake region and is diffused towards the minimum flow cross sectional area. As seen in Fig. 12, the variation in the Reynolds shear stress profiles demonstrates some weak dependence on the Reynolds number.

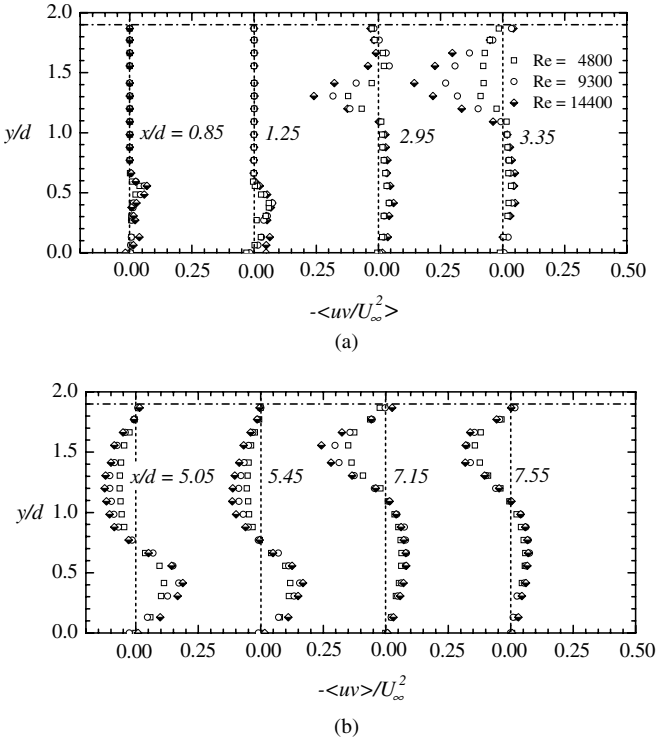

Fig. 12. Profiles of non-dimensional Reynolds shear stress, $-\langle uv\rangle/U_\infty^2$ at selected x/d locations.

3.5. Correlation coefficient and Reynolds stress ratios

The correlation coefficient, ρ_{uv}, which takes values between −1 and 1, provides a measure of the efficiency of turbulent mixing (Jovic, 1996). A positive correlation implies that when u is positive, v is likely to also be positive, and vice versa. A negative correlation implies that it is likely that the fluctuations have different signs. Fig. 13 shows the distribution of ρ_{uv} at selected x/d locations. The x-axis range is from 0.0 to 2.0 for each repeated section. These results show that ρ_{uv} is relatively low in the first row compared to the other rows. The trends in ρ_{uv} profiles are qualitatively the same beyond the second row. They have double peaks of approximately −0.5 and 0.5. This is a departure from a typical boundary layer profile, which has a single peak. The peak value is also higher than typical values reported for classical turbulent boundary layers. From these results, it can be inferred that efficient mixing occurs in the region where flow becomes spatially periodic (i.e., $x/d \geqslant 5.05$). The figure also reveals no significant change in the distribution of the correlation coefficient with Reynolds numbers.

The Reynolds stress ratios $-\langle uv\rangle/u^2$, $-\langle uv\rangle/v^2$ and v^2/u^2 ratios provide a rough indication of departure of the Reynolds stresses from isotropy. Figs. 14 and 15 show the distributions of $-\langle uv\rangle/u^2$ and $-\langle uv\rangle/v^2$, respectively, at selected x/d locations. The x-axis range for the repeated sections in these figures is 0–2. The profiles in both figures are similar both qualitatively and quantitatively to that of the correlation coefficient discussed earlier in this section.

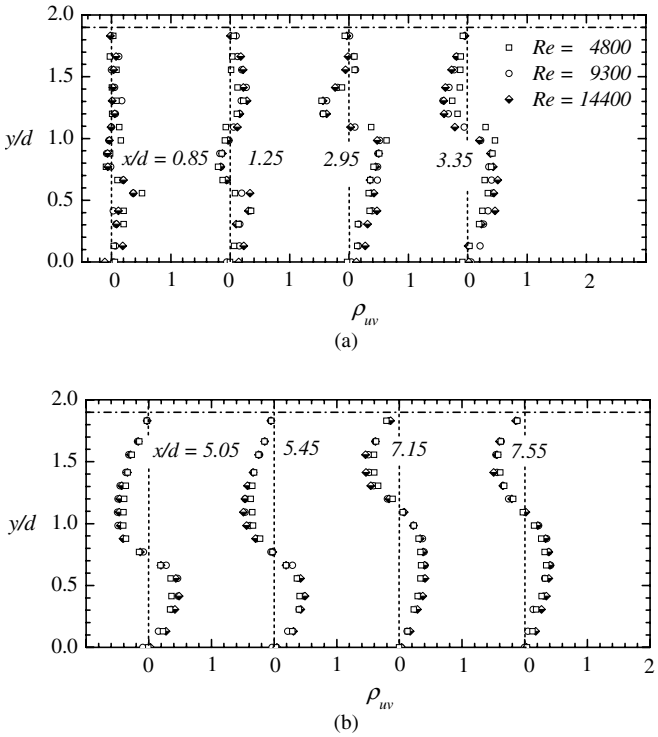

Fig. 13. Profiles of correlation coefficient, $\rho_{uv} = \langle uv\rangle/\sqrt{u^2}\sqrt{v^2}$ at selected x/d locations.

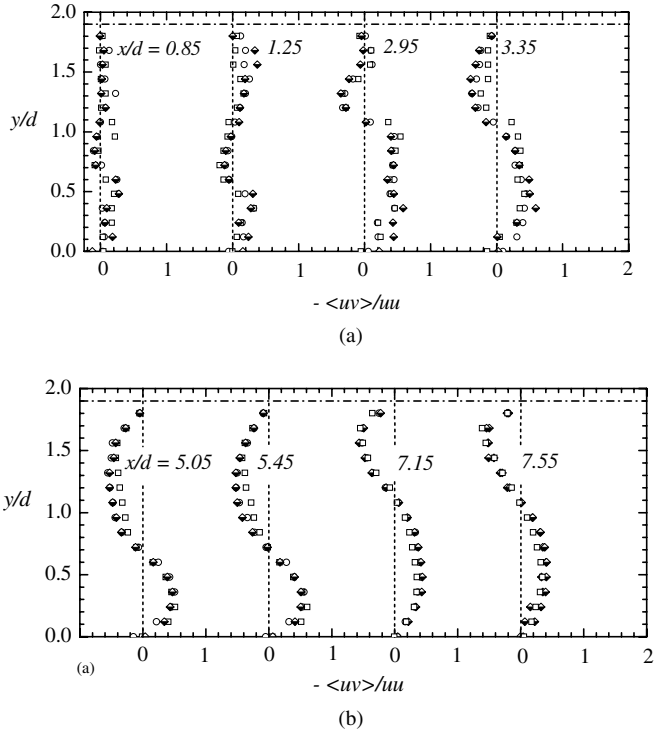

Fig. 14. Profiles of shear stress to streamwise intensity ratio, $-\langle uv\rangle/u^2$ at selected x/d locations; symbols same as in Fig. 13.

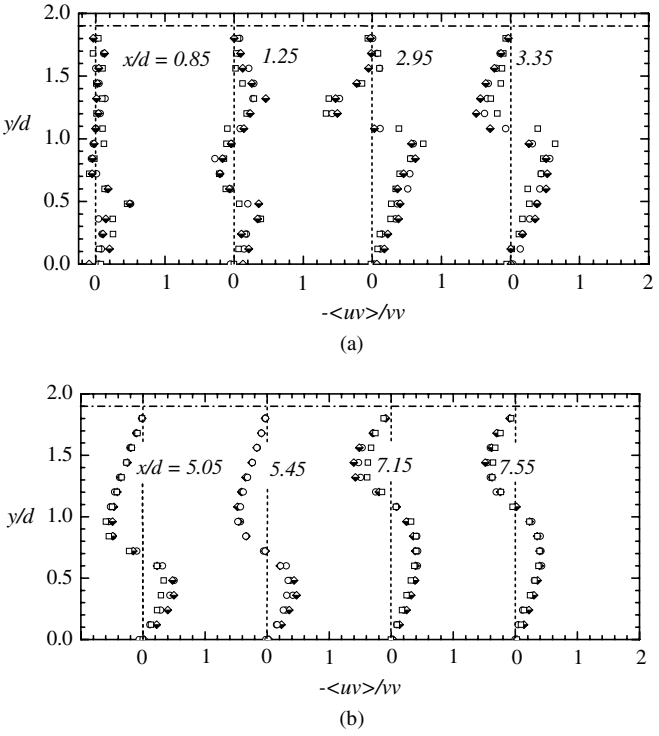

Fig. 15. Profiles of shear stress to transverse intensity ratio, $-\langle uv\rangle/v^2$ at selected x/d locations; symbols same as in Fig. 13.

As expected, the data show that the shear stresses are lower than the normal stresses.

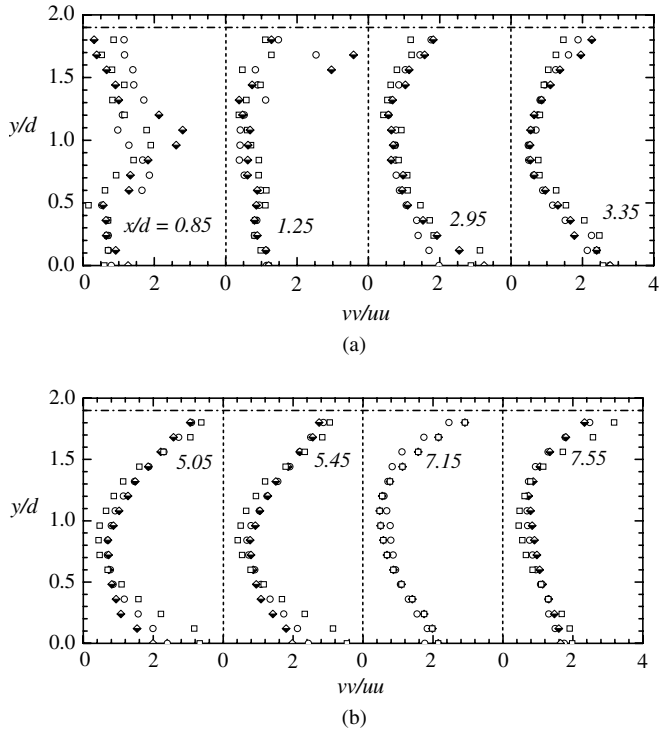

Fig. 16. Profiles of turbulence intensities ratio, v^2/u^2 at selected x/d-locations; symbols same as in Fig. 13.

The profiles of v^2/u^2 at selected x/d locations are shown in Fig. 16. The x-range of the repeated sections in this figure is 0–4. Starting from the first row (i.e., at $x/d = 0.85$ and 1.25) the magnitude of v^2/u^2 is greater than unity over much of the region. This is at variance with classical turbulent boundary layers where v^2/u^2 is generally lower than unity. From these results, it can be inferred that the flow through a tube bundle is anisotropic. The results also suggest that the enhanced turbulent mixing observed in the tube bundles does not necessarily promote stress isotropy. The profiles reveal a weak Reynolds number dependence of the Reynolds stress ratios.

3.6. Reynolds-Averaged Navier–Stokes equations

The Reynolds-Averaged Navier–Stokes (RANS) equations provide insight into the momentum transport. For steady and incompressible flow, the two-dimensional RANS equations in the streamwise and transverse direction may, respectively, be written in the following form:

$$\underbrace{\left(\frac{U\partial U}{\partial x}+\frac{V\partial U}{\partial y}\right)}_{I_x}-\underbrace{\left\{\nu\left(\frac{\partial^2 U}{\partial x^2}+\frac{\partial^2 U}{\partial y^2}\right)\right\}}_{II_x}+\underbrace{\left(\frac{\partial\langle uu\rangle}{\partial x}+\frac{\partial\langle uv\rangle}{\partial y}\right)}_{III_x}=\underbrace{\left(-\frac{1}{\rho}\frac{\partial P}{\partial x}\right)}_{IV_x} \quad (1)$$

$$\underbrace{\left(\frac{U\partial V}{\partial x}+\frac{V\partial V}{\partial y}\right)}_{I_y}-\underbrace{\left\{\nu\left(\frac{\partial^2 V}{\partial x^2}+\frac{\partial^2 V}{\partial y^2}\right)\right\}}_{II_y}+\underbrace{\left(\frac{\partial\langle uv\rangle}{\partial x}+\frac{\partial\langle vv\rangle}{\partial y}\right)}_{III_y}=\underbrace{\left(-\frac{1}{\rho}\frac{\partial P}{\partial y}\right)}_{IV_y} \quad (2)$$

where

I_x, I_y = convective term in the x and y directions, respectively;
II_x, II_y = viscous term in the x and y directions, respectively;
III_x, III_y = Reynolds stresses gradient term in the x and y directions, respectively;
IV_x, IV_y = pressure gradient term in the x and y directions, respectively.

The terms I_x, I_y to IV_x, IV_y have been made dimensionless by multiplying each term by tube diameter divided by the square of the approach velocity and are presented as I_x^*, I_y^* to IV_x^*, IV_y^*, respectively. The convective, viscous and Reynolds stresses terms in both Eqs. (1) and (2) were estimated directly from the measured data. The pressure gradient terms were obtained from the remainder required to balance the equations (i.e., $IV = I - II + III$). The profiles of the various terms in the streamwise and transverse directions at selected x/d locations are, respectively, shown in Figs. 17 and 18 for $Re_\infty = 9300$. The x-axis range of repeated sections in both figures is 0–5. It was observed that $\partial\langle uv\rangle/\partial y$ is higher than $\partial\langle uu\rangle/\partial x$ so that most of the contribution to the Reynolds stress terms in the streamwise RANS equation comes from $\partial\langle uv\rangle/\partial y$. For the transverse RANS equation, it was found that $\partial\langle uv\rangle/\partial x$ is negligibly

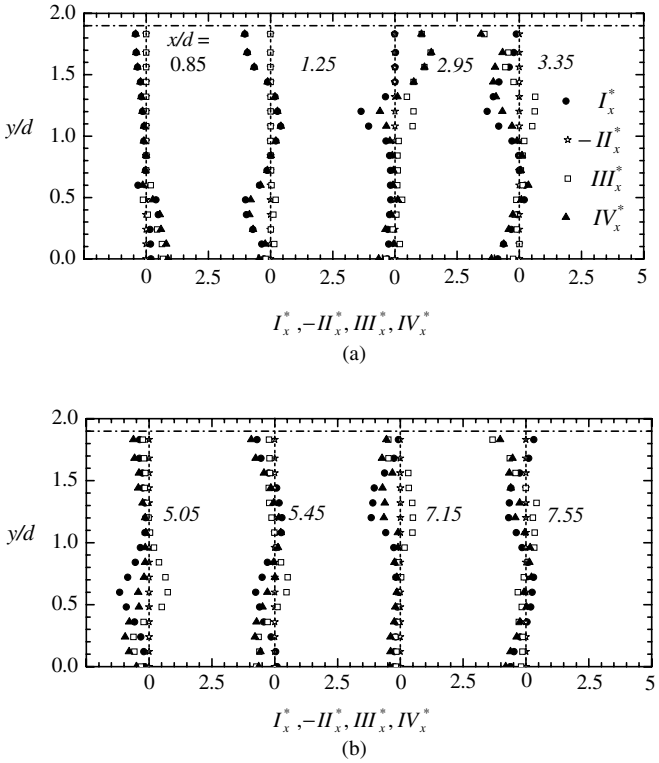

Fig. 17. Profiles of momentum transport terms in the streamwise direction (defined in Eq. (1)) normalized by $\frac{U_\infty^2}{d}$.

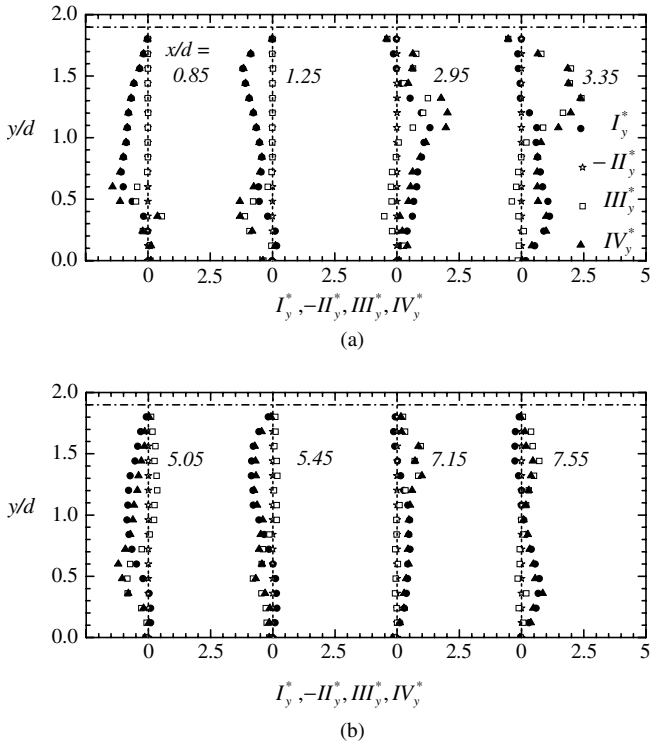

Fig. 18. Profiles of momentum transport terms in the transverse direction (defined in Eq. (2)) normalized by $\frac{U_\infty^2}{d}$.

small compared to $\partial\langle vv\rangle/\partial y$. The relative contribution of $V\partial U/\partial y$ and $U\partial U/\partial x$ to the convective term in the streamwise RANS equation varies from region to region. In the region next to the recirculation zone, for example, $U\partial U/\partial x$ is small compare to $V\partial U/\partial y$. On the other hand, $U\partial U/\partial x$ exceeds $V\partial U/\partial y$ in the minimal flow cross-sectional areas due to the strong acceleration (i.e., high $\partial U/\partial x$ values) that occur in these regions. In the case of the transverse RANS equation, it was observed that $V\partial V/\partial y$ is higher than $U\partial V/\partial x$ everywhere.

Figs. 17 and 18 clearly reveal that the viscous terms in both the streamwise and transverse RANS equations are negligibly small compared to the overall convective and Reynolds stress terms. The level of Reynolds stress terms in the streamwise and transverse RANS equations is high in the recirculation region and relatively low outside the recirculation region. The convective terms, on the other hand, are significant outside the recirculation zones and nearly negligible in the recirculation zones notwithstanding the characteristic strong shear layer and steep velocity gradients in the recirculation zones. As a result, the pressure gradient terms are nearly balanced by the Reynolds stresses in the recirculation regions, and by the convection terms outside the recirculation zones. It is also noteworthy that the transport terms in the transverse RANS equation are generally higher than corresponding terms in the streamwise equation. This observation is at variance with classical turbulent boundary layers where momentum transport in the transverse direction is negligible.

4. Conclusions

A particle image velocimetry technique was used to perform detailed measurements in turbulent cross-flow in a staggered tube bundle. The results reveal a pair of large and intense vortices behind the first row. The size and intensity of the vortices formed behind the second row of tubes are markedly diminished and disappear altogether further downstream. The flow field is characterized by high turbulence levels and intense mixing. In the recirculation zones, for example, values of the turbulence intensities are nearly as high as the approach velocity.

As a result of the enhanced turbulence levels, the flow develops very rapidly through the tube bundle and becomes spatially periodic at a relatively short distance ($x/d = 3.35$) into the tube bundle. In the developing region (i.e., $x/d \leqslant 3.35$), the turbulent profiles exhibit significant Reynolds number effects. Furthermore, significant discrepancies exist between the present data at $Re_\infty = 9300$ and the LDA measurements of Balabani and Yianneskis (1996) at a similar Reynolds number and in a tube bundle with similar pitch ratios. In the spatially periodic region ($x/d > 3.35$), on the other hand, the flow is nearly independent of Reynolds number and the present data compare very well with the measurements of Balabani and Yianneskis (1996).

Momentum balance estimates at several streamwise locations show that the viscous term can be neglected everywhere in the flow field. It was observed that the convective term is negligible in the recirculation regions, and the pressure gradient term in this region is balanced by the Reynolds stress term. Outside the recirculation zone, the Reynolds stress term is small compared with the convective term and the pressure gradient term is balanced by the latter. The results also show that momentum transport terms in the transverse direction exceed those in the streamwise direction.

Most of the Reynolds stresses are produced in the recirculation zones where the level of shear is also high, and diffused outwards. The flow is strongly anisotropic over most of the regions due to higher production of the transverse Reynolds normal stress.

Acknowledgements

The authors would like to acknowledge the support of the Natural Sciences and Engineering Research Council of Canada (NSERC) and the Canada Foundation for Innovation (CFI) for their financial support for this work.

References

Aiba, S., Tsuchida, H., Ota, T., 1982a. Heat transfer around tubes in in-line tube banks. Bull. JSME 25, 919–926.

Aiba, S., Tsuchida, H., Ota, T., 1982b. Heat transfer around tubes in staggered tube banks. Bull. JSME 25, 527–533.

Balabani, S., 1996. An experimental investigation of the cross-flow over tube bundles, Ph.D. thesis, King's College, London.

Balabani, S., Yianneskis, M., 1996. An experimental study of the mean flow and turbulence structure of cross-flow over tube bundles. Proc. IMechE C: J. Mech. Eng. Sci. 210 (4), 317–331.

Balabani, S., Bergeles, G., Burry, D., Yianneskis, M., 1994. Velocity characteristics of the cross-flow over tube bundles. In: International Proceedings of the Seventh International Symposium on Application of Laser Anemometry to Fluid Mech., vol. 2, Lisbon, pp. 39.3.1–39.3.8.

Beale, S.B., Spalding, D.B., 1999. A numerical study of unsteady fluid flows in in-line and staggered tube banks. J. Fluid Struct. 13, 723–754.

Coleman, H.W., Steele, W.G., 1995. Engineering Application of Experimental Uncertainty Analysis. AIAA J. 33, 1888–1896.

Forliti, D.J., Strykowski, P.J., Debatin, K., 2000. Bias and precision of digital particle image velocimetry. Exp. Fluids 28, 436–447.

Grimson, E., 1937. Correlation and utilization of new data on flow resistance and heat transfer for cross-flow over tube banks. ASME Trans. 59, 583.

Halim, M.S., 1988. Detailed velocity measurement of flow through staggered and in-line tube banks in cross-flow using laser Doppler anemometry. Ph.D.Thesis, University of Manchester.

Hinze, J.O., 1975. Turbulence. McGraw-Hill, New York.

Huge, E., 1937. Experimental investigation on the effect of equipment size of heat transfer and flow resistance in cross-flow of gas over tube bank. ASME Trans. 59, 573–582.

Iwaki, C., Cheong, K.H., Monji, H., Matsui, G., 2004. PIV measurement of the vertical cross-flow structure over tube bundles. Exp. Fluids l.37, 350–363.

Jovic, S., 1996. An experimental study of a separated/reattached flow behind a backward-facing step. $Re_h = 37{,}000$. NASA Technical Memorandum 110384.

Launder, B.E., Reece, G.J., Rodi, W., 1975. Progress in the development of a Reynolds Stress turbulence closure. J. Fluid Mech. 68, 537–566.

Leschziner, M.A., 2006. Modelling turbulent separated flow in the context of aerodynamic applications. Fluid Dyn. Res. 38, 174–210.

Meyer, K.E., 1994. Experimental and numerical investigation of turbulent flow and heat transfer in staggered tube Bundles. Ph.D. Thesis, Technical University of Denmark.

McKillop, A.A., Durst, F., 1984. LDA experiments of separated flow behind a circular cylinder. In: Proceedings of the Second International Symposium on Application of Laser Anemometry to Fluid Mechanics, paper 14.4.

Pierson, O., 1937. investigation of influence of tube arrangement on convection heat transfer and flow resistance in cross-flow of gases in tube banks. ASME Trans. 59, 563–572.

Polak, D.R., Weaver, D.S., 1995. Vortex shedding in normal triangular tube arrays. J. Fluids Struct. 9, 1–17.

Prasad, A.K., Adrian, R.J., Landreth, C.C., Offutt, P.W., 1992. Effect of resolution on the speed and accuracy of particle image velocimetry interrogation. Exp. Fluids l3, 105–116.

Rollet-Miet, P., Laurence, D., Ferziger, J., 1999. LES and RANS of turbulent flow in tube bundles. Int. J. Heat Fluid Flow 20, 241–254.

Simonin, O., Barcouda, M., 1986. Measurement of fully developed turbulent flow across tube bundle. In: Proceedings of the Third International Symposium on Applications of Laser Anemometry to Fluid Mech., Lisbon, Portugal.

Simonin, O., Barcouda, M., 1988. Measurement and prediction of turbulent flow entering a staggered tube bundle. In: Proceedings of the Fourth International Symposium on Applications of Laser Anemometry to Fluid Mech., Lisbon, Portugal.

Sweeney, C., Meskell, C., 2002. Numerical simulation of vortex shedding in tube arrays. In: Proceedings of IMECE 2002, ASME Int. Mech. Eng., Congress and Exposition. New Orleans, Louisiana.

Wallis, R.P., 1939. A photographic study of fluid flow between bank of tubes. Proc. IMechE 142, 379–387.

Weaver, D.S., Abd-Rabbo, A., 1985. A flow visualization study of a square array of tubes in water cross-flow. J. Fluid Eng. 107, 354–363.

Westerweel, J., 1997. Fundamental of digital particle image velocimetry. Meas. Sci Technol. 8, 1379–1392.

Žukauskas, A., Ulinskas, R., 1998. Banks of plain and finned tubes. In: Hewitt, G.F. (Ed.), Heat Exchanger Design Handbook. HEDH, New York, pp. 2.2.4-1–2.2.4-17.